Separation Science and Technology
Publication details, including instructions for authors and subscription information:
http://www.informaworld.com/smpp/title~content=t713708471

Membrane Morphology—A Model Correlating Thickness of Membrane Surface Skin Layer with Solvent Evaporation Time

Y. Wang[a]; Wayne W. Y. Lau[a]; S. Sourirajan[a]
[a] DEPARTMENT OF CHEMICAL ENGINEERING, NATIONAL UNIVERSITY OF SINGAPORE REPUBLIC OF SINGAPORE,

To cite this Article Wang, Y. , Lau, Wayne W. Y. and Sourirajan, S.(1995) 'Membrane Morphology—A Model Correlating Thickness of Membrane Surface Skin Layer with Solvent Evaporation Time', Separation Science and Technology, 30: 2, 189 — 210
To link to this Article: DOI: 10.1080/01496399508015833
URL: http://dx.doi.org/10.1080/01496399508015833

SEPARATION SCIENCE AND TECHNOLOGY, **30**(2), pp. 189–210, 1995

Membrane Morphology—A Model Correlating Thickness of Membrane Surface Skin Layer with Solvent Evaporation Time

Y. WANG, WAYNE W. Y. LAU, and S. SOURIRAJAN
DEPARTMENT OF CHEMICAL ENGINEERING
NATIONAL UNIVERSITY OF SINGAPORE
REPUBLIC OF SINGAPORE

ABSTRACT

A simple model has been developed which relates membrane surface skin layer thickness to solvent evaporation time. This model can be used to determine other important membrane morphology parameters such as pore number (or pore density) in every pore size distribution on the membrane surface. With pore number becoming available, membrane morphology can now be more completely, explicitly, and quantitatively characterized. The changes in membrane morphology parameters during the solvent evaporation step of making cellulose acetate butyrate (CAB) membrane (in acetone) were investigated based on the Surface Force-Pore Flow (SFPF) model and a new model developed in this work. The analyses show that in the solvent evaporation step of making CAB membranes, there exist three distinct morphology stages or phases associated with solvent evaporation time: (I) intrinsic pore-determining phase, (II) phase of forming dominantly massive small pores, and (III) phase of forming dominantly large pores. It is the combined effect of several morphology parameters that determines the membrane performance, which in this case yields a high solute separation and permeate rate when solvent evaporation time is set at 60 seconds.

INTRODUCTION

In the Surface Force-Pore Flow (SFPF) model developed by Sourirajan and Matsuura (1, 2) for reverse osmosis transport, membrane morphology

is characterized in terms of pure water permeation rate (PWP) and a set of parameters specifying the pore size and pore size distribution on the membrane surface. This characterization will be more complete if the number of pores (or pore density) and the thickness of membrane surface skin layer are known because they are important membrane morphology parameters which affect membrane performance.

It is well known that a thin dense surface skin layer offers lower resistance to fluid flow through the membrane. The porous substructure underneath the surface skin layer functions solely as a mechanical support for the skin. Therefore, membrane performance is generally determined by the morphology of the membrane surface skin layer. In this work a model is developed which correlates the surface skin layer thickness with solvent evaporation time in the solution casting process. This model is then used to determine another important parameter of membrane morphology—number of pores (or pore density) in every distribution on the membrane surface. In this model membrane morphology can be quantitatively characterized by the following parameters: average pore size, pore size distribution standard deviation, pore density in every distribution on the membrane surface, and thickness of the membrane surface skin layer.

The membrane studied in this work is cellulose acetate butyrate (CAB) membrane which was first investigated for reverse osmosis (RO) separation by Sourirajan (3) in 1958. Although some work had been done on CAB membranes (4–11), very few studies have been made on the morphology of this type of membrane.

Wydeven and Leban demonstrated that CAB membrane is asymmetric (7). The skin thickness of RO membrane was reported to be in the order of 0.25 to 10 μm (12–14). Anderson et al. mathematically analyzed factors influencing the skin thickness of asymmetric RO membranes (15). Ohya et al. observed that CAB membrane has large fingerlike cavities for short solvent evaporation time and dense structure for long solvent evaporation time (16). Similar observations were also made by Lu et al. (11).

It was pointed out that the solvent evaporation step has a significant effect on CAB membrane performance (1, 16–18). For example, Ohya et al. observed that pure water flux through the membrane increased with an increase in solvent evaporation time (1, 16, 17). Tweddle and Sourirajan found that solute separation by unshrunk cellulose acetate (CA) membranes gelled in 28.5% ethyl alcohol–water showed a maximum at 60 seconds solvent evaporation time (1, 18). We previously pointed out that changes in surface morphology of CAB membranes in the solvent evaporation step could be divided into three distinct stages or phases (19), but only a qualitative discussion was given. In this paper quantitative discussions will be offered to analyze the cause–effect changes during the solvent evaporation period using a model developed in this work.

THEORY

The Model

During the solvent evaporation step in a membrane-making process, solvent loss occurs only at the membrane surface; the more the solvent loss, the thicker the membrane surface skin layer becomes. We assume that the thickness of the surface skin layer of a membrane is directly proportional to the quantity of solvent evaporated during the solvent evaporation step, that is:

$$\delta \propto (W_0 - W_t) \tag{1}$$

or

$$\delta = a'(W_0 - W_t) \tag{2}$$

where δ is the thickness of the surface skin layer, W_t is the total weight of membrane and casting plate at any time t after casting, W_0 is the extrapolated value of W_t at time $t = 0$, and a' is a proportionality constant.

Solvent loss is a function of evaporation time, and this relation can be determined experimentally using the solvent loss versus evaporation time curve. The early stages of evaporation during film formation follow a relation (17, 18):

$$(W_t - W_\infty) = (W_0 - W_\infty)e^{-bt} \tag{3}$$

where W_∞ is the value of W_t at the time when solvent loss has practically ceased, and "b" is the evaporation rate constant.
Rearranging Eq. (3) yields

$$W_t = W_\infty + (W_0 - W_t)e^{-bt} \tag{4}$$

Putting Eq. (4) into Eq. (2) yields the following equation:

$$\delta = a[1 - e^{-bt}] \tag{5}$$

where

$$a = a'(W_0 - W_\infty) \tag{6}$$

Since a', W_0, and W_∞ are all constants, a is also a constant.

Equation (5) bears no reference to membrane type or membrane materials, so it is a general law applicable to any membranes made using the solution casting method. But it should be noted that this relation is applicable only to the evaporation stages corresponding to the linear portion of the solvent evaporation rate curve, as shown by an example in Fig. 1.

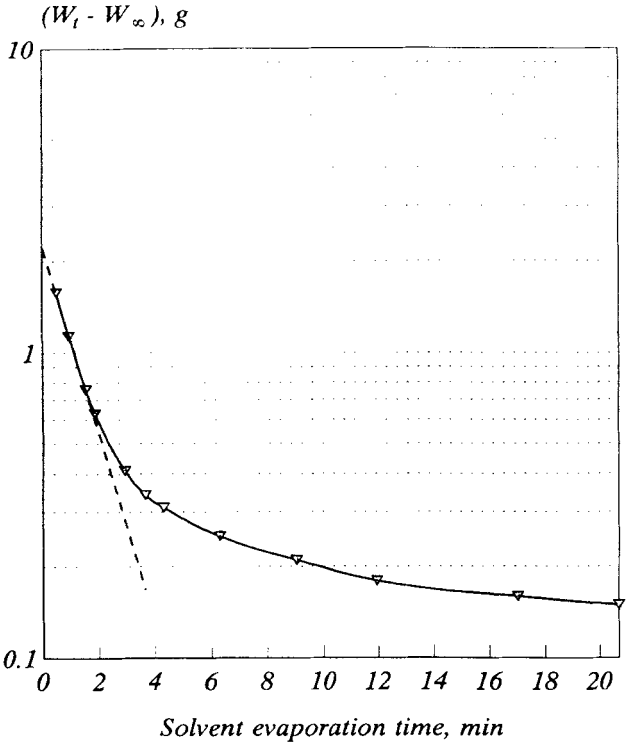

FIG. 1 Solvent evaporation rate curve. Membrane area: 430 cm^2. Temperature: 23°C.

Calculation of Pore Density in Every Pore Size Distribution on the Membrane Surface

To calculate the pore density in every pore size distribution on a membrane surface, we make use of the assumption of Sourirajan (1, 2) that the pores in the surface skin layer are cylindrical. It can be verified that liquid flow through the pores in the surface skin layer is laminar. Compared to the resistance of the surface skin layer, the resistance of the porous substructure underneath the surface skin layer is negligible for an asymmetric membrane. The Hagen–Poiseuille law can now be applied to liquid flow through the pores:

$$q = \frac{\pi \rho P \overline{R}^4}{8 \eta \delta} \tag{7}$$

where q is liquid permeation rate through *one* pore, ρ is density of liquid,

$\overline{R}$ is average radius of pores, P is operating pressure (gauge), η is viscosity of liquid; and δ is thickness of the membrane surface skin layer.

Defining N_i as number of pores in the ith distribution on a given area of membrane surface, then

$$\text{PWP} = \sum_{i=1}^{n} N_i q_i \tag{8}$$

where PWP is the amount of pure water permeated through a given area of membrane surface, n is the number of pore size distributions on the membrane surface, and q_i is the pure water flux through one pore in the ith distribution.

Define:

$$h_i = N_i/N_1 \tag{9}$$

or

$$N_i = h_i N_1 \tag{10}$$

Putting Eq. (10) into Eq. (8):

$$\text{PWP} = \sum_{i=1}^{n} h_i N_1 q_i \tag{11}$$

$$= N_1 \sum_{i=1}^{n} (h_i q_i) \tag{12}$$

Combining Eqs. (12) and (7) and rearranging yields the following equation:

$$N_1 = \frac{8\eta\delta\text{PWP}}{\pi\rho P \sum_{i=1}^{n} (h_i \overline{R}_{b,i}^4)} \tag{13}$$

where $\overline{R}_{b,i}$ is the average radius of pores in the ith distribution on the membrane surface. $\overline{R}_{b,i}$ and h_i are calculated using the SFPF model (1, 2).

Once N_1 is obtained, N_i can be determined using Eq. (10).

The above equations can be used to calculate the number of pores in any distribution for any number of pore size distributions on the membrane surface. For a membrane with only one pore size distribution, the number of pores is determined using the following equation:

$$N = \frac{8\eta\delta\text{PWP}}{\pi\rho P \overline{R}_b^4} \tag{14}$$

where N is the total number of pores and $\overline{R}_b$ is the average radius of pores on the membrane surface.

For a membrane with two pore size distributions:

$$N_1 = \frac{8\eta\delta\text{PWP}}{\pi\rho P(\overline{R}_{b,1}^4 + h_2\overline{R}_{b,2}^4)} \tag{15}$$

where $\overline{R}_{b,1}$ and $\overline{R}_{b,2}$ are average radii of pores in the first and second pore size distributions, respectively, and h_2 is the pore number ratio of the second to the first distribution.

Defining N as the total number of pores of all pore sizes on a given area of membrane surface, then

$$N = \sum_{i=1}^{n} N_i \tag{16}$$

And defining Q_i as the quantity of membrane permeated water and β_i as the fraction of total water permeated through the pores in the ith pore size distribution, then

$$\text{PWP} = \sum_{i=1}^{n} Q_i \tag{17}$$

$$Q_i = N_i q_i \tag{18}$$

$$\beta_i = Q_i/\text{PWP} \tag{19}$$

and

$$\sum_{i=1}^{n} \beta_i = 1 \tag{20}$$

Let S be the effective membrane surface area, $\bar{n}_i$ be the pore density of the ith pore size distribution, and $\bar{n}$ be the overall pore density, then

$$\bar{n}_i = N_i/S \tag{21}$$

$$\bar{n} = \sum_{i=1}^{n} \bar{n}_i \tag{22}$$

or

$$\bar{n} = N/S \tag{23}$$

and

$$Q_i = S\bar{n}_i q_i \tag{24}$$

EXPERIMENTAL

Membrane Making

Cellulose acetate butyrate [CAB-17-15, butyryl content: 17%, viscosity (ASTM): 15 seconds] membranes of different surface morphologies were made in the laboratory according to the following procedures (6): All the ingredients of a membrane casting solution were thoroughly mixed by a MDC-NR stirrer. The casting solution was cast onto a flat glass plate using a casting bar made of brass. The film on the glass plate was exposed to the atmosphere at ambient temperature for a desired time period and then quenched in an ice-water bath initially at 0 to 2°C. The gelation bath temperature rose gradually to room temperature during the immersion period of at least overnight duration. The film was washed with a large amount of water to thoroughly remove the solvent and additives in the membrane prior to using it in RO experiments. The composition of the CAB membrane casting solution and details of membrane making in this work are summarized in Table 1. CAB was obtained from Eastman Kodak Company. Triethyl phosphate, lactic acid, and glycerol were supplied by Merck.

Membrane Cell

Thin channel ultrafiltration flow cells were used in this work. They are of the same design as those used by Sourirajan (1) except that the effective area of the membrane used in each cell was 18.06 cm^2. Since the membrane permeated product rate (PR) from each cell was usually much smaller than the feed flow, the difference in the concentrations of the feed solution

TABLE 1
Film Casting Conditions

Composition of casting solution, wt%:	
CAB-17-15	15
Triethyl phosphate	23
Glycerol	2
Lactic acid	6
Acetone	54
Temperature of casting solution, °C	23–24
Temperature of casting environment, °C	23–24
Gelation medium	Ice-cold water
Gelation bath temperature, °C	0–2
Period of leaching membrane in gelation bath	Overnight (≥15 h)
Film casting tool	Polished brass casting bar

entering and leaving a cell on the high pressure side of the membrane was negligible. Feed concentrations in all cells were considered unchanged.

All membranes were initially subjected to a pressurization treatment to stabilize their porous structures. Aqueous NaCl solutions were used for membrane characterization. Concentrations of NaCl in feed and product streams were determined using a Horiba Conductivity Meter ES-14. In each experiment the following data were collected: pure water permeation rate (PWP), permeated product rate (PR) in g/h, and solute separation f. The PWP and PR data were corrected to 25°C using the viscosity data of pure water.

Membrane performance is expressed in terms of PR (in g/h per given area of membrane) and f defined as

$$f = \frac{(\text{ppm solute in feed}) - (\text{ppm solute in product})}{(\text{ppm solute in feed})} \tag{25}$$

The SFPF model (1, 2) was used to determine membrane morphology parameters—pore size, pore size distribution, and pore number ratio. The reference solutes chosen to determine these parameters were a series of crown ethers with similar chemical structures but different molecular weights. Their properties are shown in Table 2. The feed concentrations of these reference solutes were about 100 ppm. A total organic carbon analyzer (Shimadzu TOC 5000) was used to determine the solute concentrations in the feed and product streams.

RESULTS AND DISCUSSION

Determination of Solvent Evaporation Rate Constant b

To determine solvent evaporation rate constant b, the solvent evaporation rate curve of CAB/acetone solution was determined experimentally

TABLE 2
Reference Solutes Used to Determine Membrane Morphology

No.	Reference solute	Molecular weight	$\mathbf{B}^a \times 10^{30}$, m^3	$\mathbf{D}^b \times 10^{10}$, m
1	1,3-Dioxolane	74.08	42.43	1.96
2	*p*-Dioxane	88.11	53.87	2.23
3	12-Crown-4	176.21	28.68	3.19
4	15-Crown-5	220.27	−321.8	3.77
5	18-Crown-6	264.32	−202.6	4.29

[a] Data for CA (1). (The **B** values for CA are assumed valid for CAB materials for the purpose of illustration.)

[b] Stokes' radius.

(see Fig. 1). From the linear portion of the curve, b was determined to be 0.6523 min^{-1}. Therefore:

$$\delta = a[1 - e^{-bt}] \tag{26}$$
$$= a[1 - e^{-0.6523t}] \ \mu m$$

Determination of Constant a. Constant a can be determined by measuring the actual thickness of the surface skin layer of a CAB membrane made at known solvent evaporation time. Scanning electron microscopy (SEM) can be used for this purpose. The cross-sectional structures of CAB membranes made under different solvent evaporation times were observed (Fig. 2) using a SEM (JEOL JSM D330A). A membrane made under short solvent evaporation time has large and long tapering fingerlike cavities (Fig 2a) which extend to the top layer, and it has a very thin top skin layer (Fig. 2b). When the solvent evaporation time is intermediate, the so-made membrane possesses independent pearshaped cavities with the stem pointing upward toward the skin layer (Fig 2c). When the evaporation time is long, a dense structure, still with a skin layer on the top, appears, but no cavities are formed (Fig. 2d). Similar results have been reported by Ohya et al. [16]. The thickness of the surface skin layer of these membranes was measured. Results are shown in Table 3.

Using the above experimental data for surface skin layer thickness δ, the value of constant a was determined using Eq. 3 (see Table 4).

Assuming that the average value of $a = 5.34$ μm is acceptable,

$$\delta = 5.34[1 - e^{-0.6523t}] \quad (\mu m) \tag{27}$$

Equation (27) quantitatively expresses a correlation between the surface skin layer thickness of CAB membranes and solvent (acetone) evaporation time. From Eq. (27) it may be seen that when the solvent evaporation time approaches zero, the surface skin layer thickness also approaches zero. But δ will not approach the value of constant a (5.34 μm in this work) when the solvent evaporation time approaches infinity because Eq. (27) is only applicable to the linear portion of the evaporation curve.

Morphology Changes during Solvent Evaporation Step

Previous experimental results of CAB membrane performance (19) showed that a maximum solute separation f_{max} exists at 60 seconds of solvent evaporation time, while the permeated product rate (PR) always increases with increasing solvent evaporation time during the whole evaporation period (see Fig. 3). Membrane performance is governed by membrane morphology. As pointed out (19) earlier, there exist three distinct morphology stages or phases in the solvent evaporation step in CAB mem-

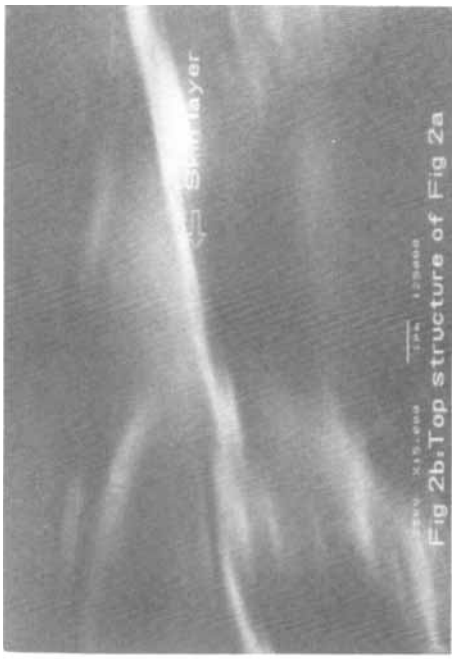

Fig 2b. Top structure of Fig 2a

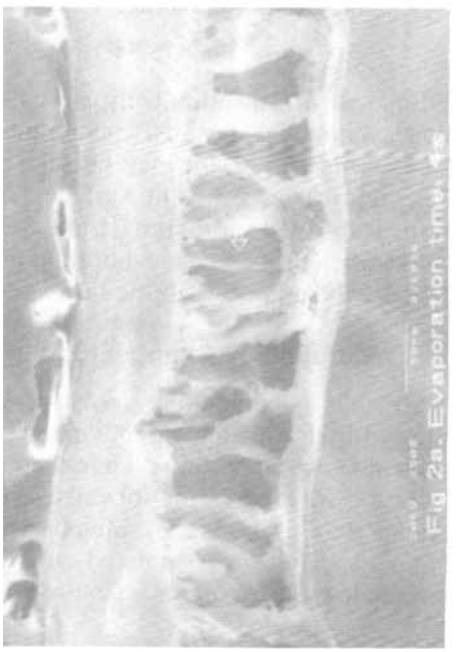

Fig 2a. Evaporation time: 4s

FIG. 2 Cross-sectional structures of CAB membranes.

TABLE 3
Thickness of the Surface Skin Layer of CAB Membranes

Membrane	Solvent evaporation time (seconds)	Surface skin layer thickness (μm)
a	4	0.25
b	60	2.6
c	150	4.3

TABLE 4
Constant a of CAB Membranes

Membrane	Solvent evaporation time		a, μm
	Seconds	Minutes	
a	4	0.067	5.24
b	60	1	5.43
c	150	2.5	5.35
			Average 5.34

brane making: 1) intrinsic pore-determining phase (phase I), 2) phase of forming massive small pores (phase II), and 3) phase of forming large pores (phase III). A qualitative analysis on these morphology changes has been given (19). In the following sections, quantitative expressions will be given to analyze these morphology changes, and hence performance, of CAB membranes in each stage.

As mentioned before, membrane morphology parameters—pore sizes, pore size distributions, and pore number ratio of two distributions—were determined based on the SFPF model (1, 2) using the reference solutes shown in Table 2, and other membrane morphology parameters—pore numbers (or pore densities) and thickness of membrane surface skin layer—were determined using the model described above.

Figure 4 shows average pore sizes in the surface layer of membranes formed at different solvent evaporation times. When the curves are extrapolated to zero solvent evaporation time, that is, when no solvent loss occurs at the cast liquid film surface, the extrapolated value may be called the "intrinsic pore size"—i.e., the size of incipient pores already existing in a casting solution by virtue of its structure. The following picture can be visualized. Macromolecules like CAB at high concentration do not

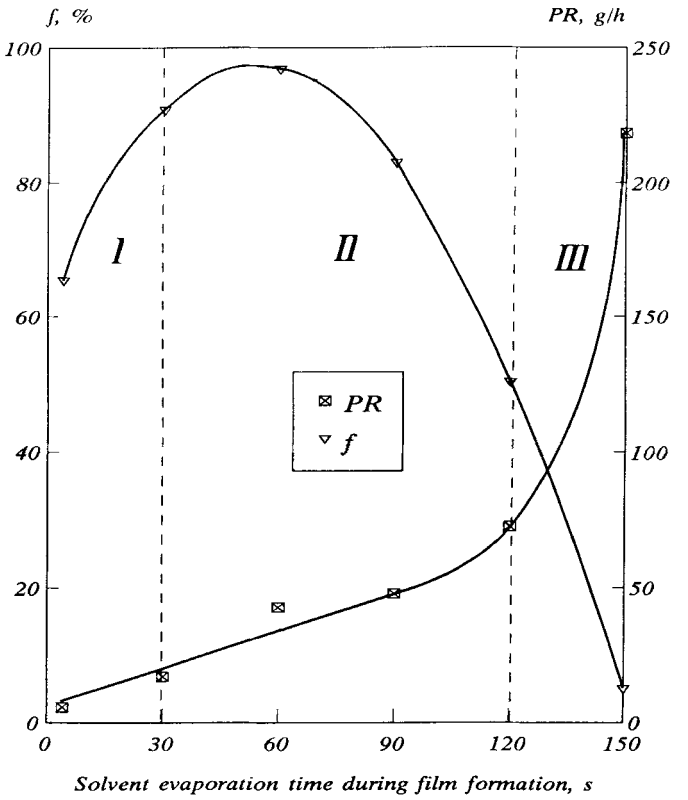

FIG. 3 Effects of solvent evaporation time on PR and f. Operating pressure: 1000 psig. Feed rate: 1200 mL/min. Feed concentration: 4850 ppm NaCl.

distribute themselves uniformly in solution. Instead they form aggregates, each consisting of a number of macromolecules entangled and overlapping each other. When these solvent-swollen aggregates come close together they form void spaces filled with a mixture of solvent and nonsolvents. According to the Solution Structure-Desolvation Rate (SSDR) approach of Sourirajan (20), the "empty" spaces within each aggregate will give rise to small pores (belonging to the first pore size distribution) and the "void" spaces formed among aggregates will give rise to larger pores (belonging to the second pore size distribution), as schematically represented in Fig. 5. These are the "intrinsic pores" which are expected to

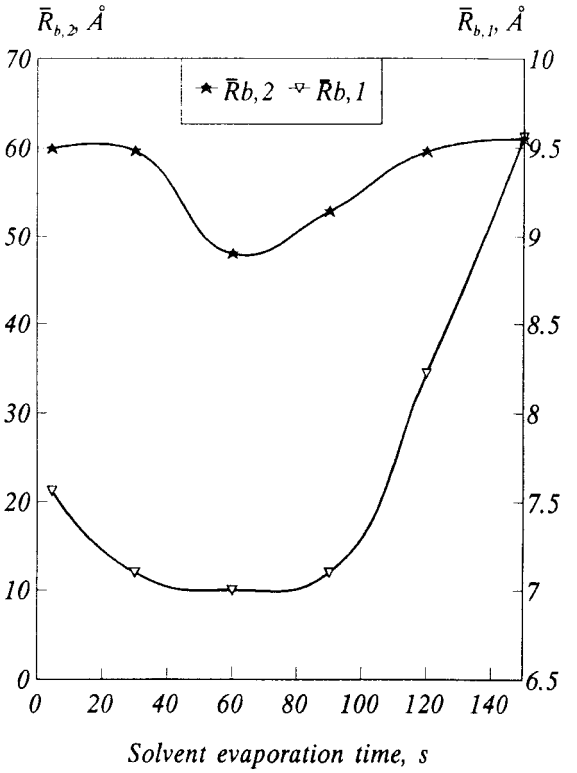

FIG. 4 Effect of solvent evaporation time on average pore size. Operating pressure: 800 psig. Feed rate: 1400 mL/min. Feed concentration: About 100 ppm for all reference solutes.

be quite uniformly distributed when they exist in the cast solution as this solution approaches closer to an equilibrium state. Once the solution is cast and solvent evaporation starts, loss of solvent from the film surface disturbs this equilibrium and the macromolecules adjust and rearrange themselves to fill the space left behind by the evaporated solvent molecules, leading to a decrease in pore size of both distributions in the surface layer of the membranes made in the initial, short solvent evaporation time (less than 60 seconds) as shown in Fig. 4. When concentration gradients, with respect to solvent, additives, and macromolecules, have developed with time to a high enough level, diffusion of the much smaller solvent and additive (thus faster) molecules from underneath the film surface layer becomes so intensive that solvent continues to move through the pores

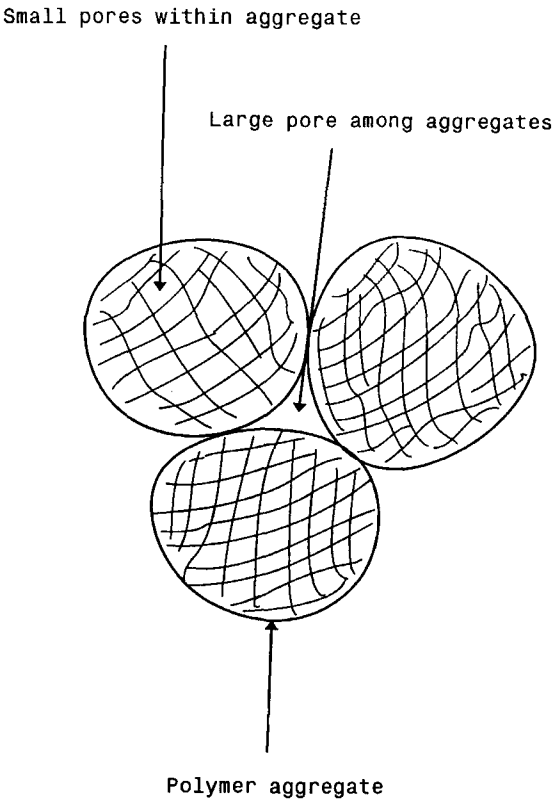

FIG. 5 Schematic representation of two types of pores.

to the membrane surface. Evaporation of the solvent then leaves behind more and more additive molecules in the membrane pores. These additive molecules are non-solvent for polymer. Their accumulation in the surface pores occupies more and more space which has to be provided by another adjustment and rearrangement exercise by the polymer molecules. This exercise is reflected in Fig. 4 by an increase in membrane pore size with solvent evaporation time. This process is stopped once the cast film is quenched in a total nonsolvent like water, whereby the membrane becomes frozen and its structure becomes fixed to a large extent. Postmembrane treatments like thermal shrinkage would allow some minor adjustment to the overall membrane morphology.

Changes in pore number are shown in Fig. 6. The number of larger pores (in the second distribution) always increases with increasing solvent

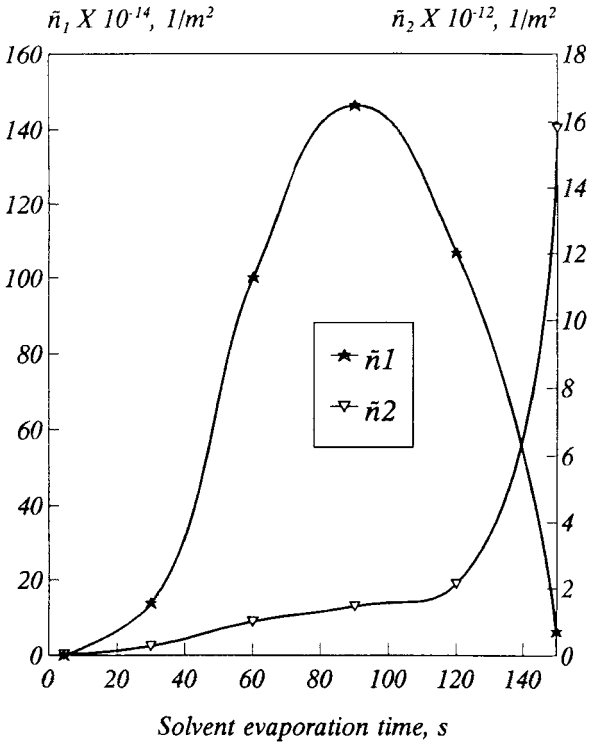

FIG. 6 Effect of solvent evaporation time on pore density. Operating pressure: 800 psig. Feed rate: 1400 mL/min. Feed concentration: About 100 ppm for all reference solutes.

evaporation time during the whole evaporation period. As pointed out earlier (19), this may be caused by the continuous formation of larger droplets of nonsolvents originating from the continuous coalescence of smaller droplets in the surface layer. On the other hand, the number of smaller pores (in the first distribution) increases first with increasing solvent evaporation time in the range shorter than 90 seconds, reaching a maximum number at 90 seconds, and then decreases after 90 seconds. Figure 7 shows changes in pore number ratio of the second to the first distribution, h_2, with solvent evaporation time. Also in Fig. 7, h_2 is indicative of the relative tendency of forming larger pores during the solvent evaporation period. The results in Figs. 6 and 7 indicate the following: 1) in phase I [when no, or little, solvent evaporation occurs (19)], both $\tilde{n}_1$ and $\tilde{n}_2$ are very low, as shown by the very low membrane permeated product rate (see phase I in Fig. 3); 2) in phase II (intermediately long

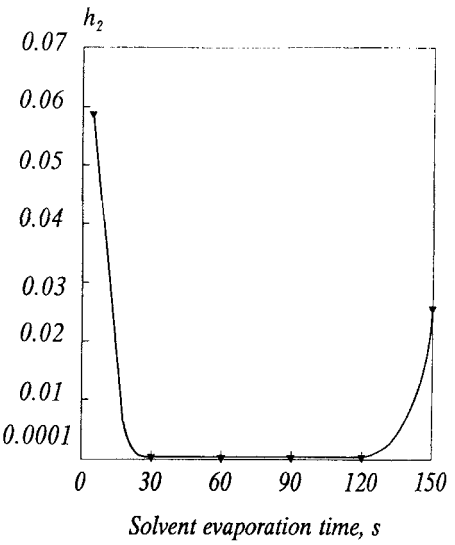

FIG. 7 Effects of solvent evaporation time on h_2. Operating pressure: 800 psig. Feed rate: 1400 mL/min.

evaporation time), $\bar{n}_2$ increases slightly but $\bar{n}_1$ increases greatly to a maximum at 90 seconds evaporation time to place h_2 at a very low level, indicating that in phase II the pore-forming rate in the first (i.e., smaller pores) distribution is much higher than that in the second (i.e., larger pores) distribution. One may visualize that this is caused by numerous small droplets of nonsolvents being formed in the surface skin layer due to diffusion and coalescence of nonsolvent molecules from the bulk solution, resulting in the formation of a large number of smaller pores. It is obvious that pore sizes and h_2 are the key factors which determine solute separation f. A maximum $\bar{n}_1$ and a smallest h_2 in phase II combine to yield a maximum f in this phase. The fact that this maximum f occurred when the smallest pores were made at an evaporation time of 60 seconds, but did not occur when the maximum number of pores were formed at 90 seconds evaporation time, indicates again that f depends on pore sizes rather than on pore number ratio h_2. Larger pores are also formed in phase II, but the formation of small pores is still dominant. This phase may be referred to as the phase for forming dominantly small pores. In phase III (long evaporation time), $\bar{n}_2$ and h_2 increase but $\bar{n}_1$ start to decrease, indicating that the formation of pores belonging to the first distribution becomes slower, and that of those in the second distribution is accelerated. Larger

$\bar{n}_2$ and h_2 values and the larger pores formed in phase III account for the low solute separation and high PR for membranes made in this phase. Phase III may be referred to as the phase for forming dominantly larger pores.

Increase in thickness of membrane surface skin layer with solvent evaporation time is shown in Fig. 8. Good agreement between the experimentally measured values and values calculated using Eq. (27) lends support to the model described above.

The relative role of pores in the first and second distribution can also be characterized by the amount of water through these pores, expressed in fractions of total water permeation, β_1 or β_2 (Fig. 9). In phase II, β_1 is much higher than β_2, while in other phases β_2 is higher than β_1. A maximum and a minimum exist for β_1 and β_2, respectively, at a solvent evaporation time of 60 seconds, indicating that in phase II the small pores belonging to the first distribution play a dominant role in determining membrane performance, and that in the other phases the bigger pores in the second distribution play a dominant role.

Pore size distribution is a relatively weaker factor which affects mainly solute separation (1, 21). Figure 10 shows the variation in pore size uniformity measured by its standard deviation (σ) divided by its mean radius

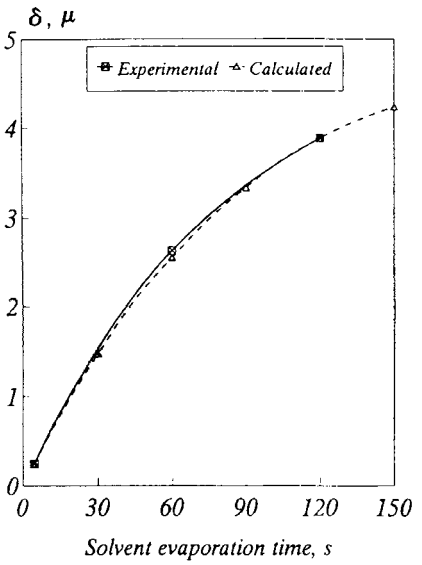

FIG. 8 Effects of solvent evaporation time on the thickness of the surface skin layer.

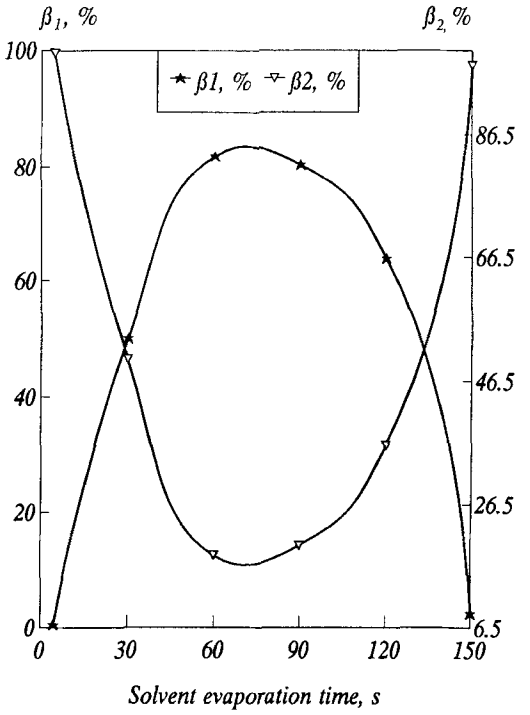

FIG. 9 Effect of solvent evaporation time on fractional flow rates. Operating pressure: 800 psig. Feed rate: 1400 mL/min. Feed concentration: About 100 ppm for all reference solutes.

($\overline{R}_b$). In phase II, one may expect that the size of pores in the surface layer should fall in the range of size of a nonsolvent molecule to the size of the largest nonsolvent droplet, and larger $\sigma_1/\overline{R}_{b,1}$ and $\sigma_2/\overline{R}_{b,2}$ should be expected in this phase (Fig. 10). In phase III, one may expect that the diffusion of nonsolvent molecules from the sublayer to the surface layer is slow or it may even cease while the coalescence of small nonsolvent droplets continues. Therefore, the pore sizes in this phase are more uniform, i.e., σ_1 and σ_2 become smaller. σ_1 and σ_2 are small (especially so for σ_2) in phase I, indicating that the pores (especially pores belonging to the second distribution) made in this phase are uniform in size as they had deviated less from the "intrinsic pores."

From the above discussion it can be clearly seen that membrane performance is determined by interactions of many parameters: pore sizes, pore size distributions, pore numbers in the distributions, as well as thickness of the surface skin layer. Any of these parameters can affect membrane

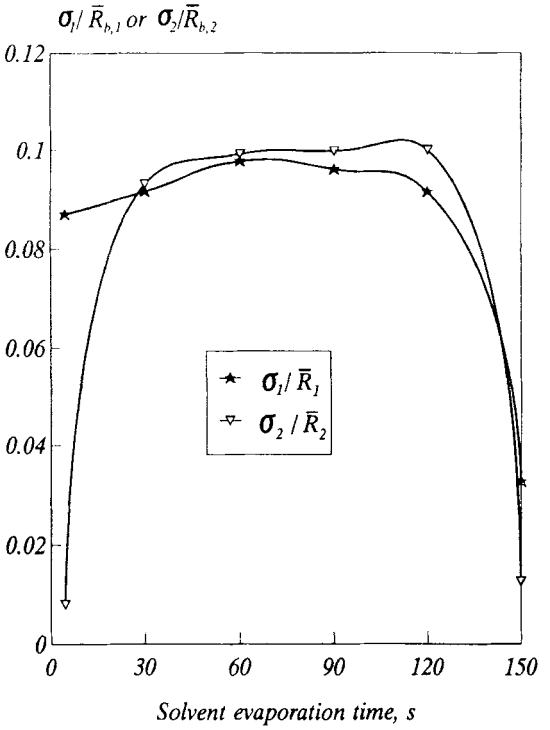

FIG. 10 Effect of solvent evaporation time on pore size distributions. Operating pressure: 800 psig. Feed rate: 1400 mL/min. Feed concentration: About 100 ppm for all reference solutes.

performance to varied extents. Apparently pore size affects both solute separation f and product permeation rate PR (or PWP) significantly (to the fourth power, Eq. 13). Pore numbers and the skin layer thickness affect PR (or PWP) only to the first power (Eq. 13). Pore size distribution affects mainly solute separation (1, 21) but to a slight extent. Therefore, the strength of influence of membrane morphology parameters appears in the following order: Pore size > pore number > membrane skin layer thickness > pore size distribution.

Based on the relative magnitudes of these morphology parameters, one may predict membrane performance under a given set of operating conditions, and conversely, these membrane morphology parameters can be determined from membrane performance data using the methods described above.

CONCLUSIONS

A general correlation relating membrane surface skin layer thickness δ to solvent evaporation time t can be expressed as

$$\delta = a[1 - e^{-bt}]$$

For CAB membranes made from CAB/acetone solution,

$$\delta = 5.34[1 - e^{-0.6523t}] \qquad (\mu m \text{ with } t \text{ in minutes})$$

δ determined using this correlation can be used to determine the number of pores or pore density in every pore size distribution using the following equations:

$$N_1 = \frac{8\eta\delta PWP}{\pi\rho P \sum_{i=1}^{n} (h_i \bar{R}_{b,i}^4)}$$

$$= h_i N_1$$

and

$$\tilde{n}_i = N_i/S$$

Thus membrane morphology can be quantitatively characterized by the following parameters: average pore size, standard deviation, pore number (or pore density) in every distribution, and thickness of the membrane surface skin layer. With these membrane morphology parameters, one can predict membrane performance under a given set of operating conditions and vice versa.

In the solvent evaporation step of making CAB membranes from a casting solution, there exist three distinct morphology stages or phases: (I) intrinsic pore-determining phase, (II) phase of forming dominantly small pores, and (III) phase of forming dominantly large pores. The interactions of these morphology parameters of CAB membranes affect and determine the membrane performance, leading to a maximum solute separation exhibited by membranes made at 60 seconds solvent evaporation time.

ACKNOWLEDGMENTS

The authors would like to express their thanks to the National University of Singapore for providing a research scholarship to Y. Wang, and to Chan Siew Weng and Tang Shu Hong for writing the computer programs for this work.

REFERENCES

1. S. Sourirajan and T. Matsuura, *Reverse Osmosis/Ultrafiltration Process Principles*, National Research Council Canada, Ottawa, 1985.
2. T. Matsuura and S. Sourirajan, *Ind. Eng. Chem., Process Des. Dev., 20*, 273 (1981).
3. S. T. Yuster and S. Sourirajan, *Report No. 58-26*, Department of Engineering, UCLA, 1958.
4. S. Manjikian, S. Liu, M. I. Foley, C. Allen, and B. Fabrick, *Progress Report No. 534*, Office of Saline Water R & D, US Department of the Interior, Washington, D.C., 1970.
5. S. Manjikian and M. I. Foley, *Progress Report No. 612*, Office of Saline Water R & D, US Department of the Interior, Washington, D.C., 1970.
6. S. Manjikian, US Patent 3,607,329 (1971).
7. T. Wydeven and M. Leban, *J. Appl. Polym. Sci., 17*, 2277 (1973).
8. J. Anderson, S. Hoffman, and C. Peters, *J. Phys. Chem., 76*, 4006 (1972).
9. H. Ohya, *J. Appl. Polym. Sci., 23*, 663 (1979).
10. H. Ohya, N. Akimoto, and Y. Negishi, *Membrane, 5*(3), 179 (1980).
11. X. Lu, Y. Liu, P. Zhou, and X. Sun, *Water Treat., 2*(1), 15 (1987).
12. R. L. Riley, J. O. Gardner, and U. Merten, *Science, 143*, 801 (1964).
13. B. Keilin, *The Mechanism of Desalination by Reverse Osmosis*, Office of Saline Water, RDPR No. 84, PB 181571, 1963.
14. U. Merten, *Desalination by Reverse Osmosis*, MIT Press, 1966.
15. J. E. Anderson and R. Ullman, *J. Appl. Phys., 44*(10), 4303 (1973).
16. H. Ohya, N. Akimoto, and Y. Negishi, *J. Appl. Polym. Sci., 24*, 663 (1979).
17. B. Kunst and S. Sourirajan, *Ibid., 14*, 2559 (1970).
18. T. A. Tweddle and S. Sourirajan, *Ibid., 22*, 2265 (1978).
19. W. Yang, W. W. Y. Lau, and S. Sourirajan, *Sep. Sci. Technol., 29*(13), 1689 (1994).
20. S. Sourirajan, *Lectures on Membrane Separation*, National Research Council Canada, Ottawa, 1991.
21. T. Matsuura, T. A. Tweddle, and S. Sourirajan, *Ind. Eng. Chem., Process Des. Dev., 23*, 674 (1984).

Received by editor April 11, 1994